Grant agreement no:	Project Acronym:	Project title:
711792	**LiRichFCC**	**Novel Cathode Materials for Lithium Ion Batteries**

Organization name of lead contractor:	Document version:
National Institute of Chemistry	**2019-03-11**

Work package:

WP 3: Dynamics of Li^+ in the material

Title:

D3.3: Porous electrode model development and verification

Start date of project:	Contractual Delivery Date:	Actual Delivery Date:
Oct. 1st 2016 **(duration 36 months)**	**2019-03-31**	**2019-03-29**

Dissemination level:

☒ **PU (Public)**

☐ **CO (Confidential, only members of the consortium + Commission)**

Authors (beneficiary name):

Dr. Jean-Marcel Ateba Mba (NIC)
Dr. Jože Moškon (NIC)
Dr. Elena Tchernychova (NIC)
Sorour Semsari Parapari (NIC)
Dr. Francisco Ruiz Zepeda (NIC)
Dr. Victoria Bracamonte (NIC)
Prof. Dr. Miran Gaberšček (NIC)
Prof. Dr. Robert Dominko (NIC)

This project has received funding from the European Union's Horizon 2020 research and innovation programme under grant agreement No 711792.

1 EXECUTIVE SUMMARY

We focused on the measurement of EIS spectra in half-cell (cathode//Li) and symmetrical cell (cathode//cathode) configurations and on physical interpretation of the obtained spectra. Three materials (Li_2VO_2F, Li_2FeO_2F and Li_2TiO_2F) were involved, all yielded by mechanosynthesis. In the first part of this report we also provide the history/background of the material that was delivered from our consortium's patterns. As shown, different parameters contribute to the measured shapes and sizes of EIS spectra such as: electrolyte concentration, electrode loading, and electrode ageing… Systematic variation of those parameters represents invaluable information for easier interpretation of the spectra.

2 INTRODUCTION

The main objective of LiRichFCC was to explore the potential of a new storage principle for lithium ions and of an associated, new class of materials for Li-ion batteries. These materials can store and reversibly exchange more than one lithium ion per formula unit by a mechanism which yields unprecedented packing densities and highest volumetric content of Li in a cathode (7500 Wh/L). The first studies have shown that oxyfluorides with the general composition Li_2MO_2F (M = V, Cr) do not store lithium through a "classical" intercalation mechanism but rather incorporate Li into their crystal structure, leading to unexpected and novel dynamics and properties.

In order to achieve this main objective, the consortium has set up different discipline plans gathered in different work packages (WP). The main goal of WP3 is to understand and optimize the charge transport in LiRichFCC materials, both in the bulk and at the interface. WP3 is divided in 3 different tasks: Dynamics of Li^+ in the material, Interfacial transport and Porous electrode model development and verification. The latter can be tackled by developing a suitable impedance model on the continuum level (i.e., a "porous electrode model").

Parameters like diffusion coefficients, charge transfer resistance, electrolyte resistance, thickness of interfacial layer, porosity, tortuosity etc. can be directly linked to impedance spectra measured under different conditions (electrolyte concentration, pressure, electrode thickness, temperature). At least in theory, such an approach allows a clear separation of different processes such as electronic and ionic wiring, transport across electrolyte/active particle interface, bulk transport.

In this interim report, attention was given to 3 different materials obtained by ball milling: Li_2VO_2F, Li_2FeO_2F and Li_2TiO_2F. Other reports related to electrochemical performance report (WP1: D1p2), transport report (WP3: D3p1) will be connect with this report in order to understand and interpret the result presented here. In this communication we summarize the progress achieved in understanding the impedance of the mentioned material.

3 DEVELOPMENT OF IMPEDANCE MODEL OF LIRICHFCC MATERIALS

3.1 Background of LiRichFCC Materials

In order to set up appropriate impedance model through the measurement EIS, and more importantly in order to understand and interpret the spectra, it is important to understand the background of the materials. In this report, we present the summary of the synthesis and properties, the electrochemical performances, dynamics of Li^+ in the material / Interfacial transport…

3.1.1 Synthesis and properties

The Li_2VO_2F compound sent to the project partners was synthesized by a simple mechanosynthesis approach involving ball milling using a Fritsch Pulverisette 6 planetary ball mill. The precursor compounds Li_2O, V_2O_3 and LiF were loaded into a Si_3N_4 milling vial with Si_3N_4 balls under argon atmosphere in a glove box. The powder mixture was milled in the sealed vial at 600 rpm for 40 h.

For Li_2FeO_2F and Li_2TiO_2F, stoichiometric amounts of Fe_2O_3 and Ti_2O_3, Li_2O (from Alfa Aesar) and LiF (from Aldrich) (total mass of ca. 5 g) were introduced into a zirconium oxide jar together with 25 balls of 10 mm of diameter. A planetary grinder from Retsch (RETSCH PM 200) was used at a rotation rate of 600 rpm (with a reverse rotation every hour) during 48 hours. Color of the recovered material was brownish and grey for Li_2FeO_2F and Li_2TiO_2F respectively. SEM image in Figure 1 reveal the approximate range of particle sizes of Li_2VO_2F.

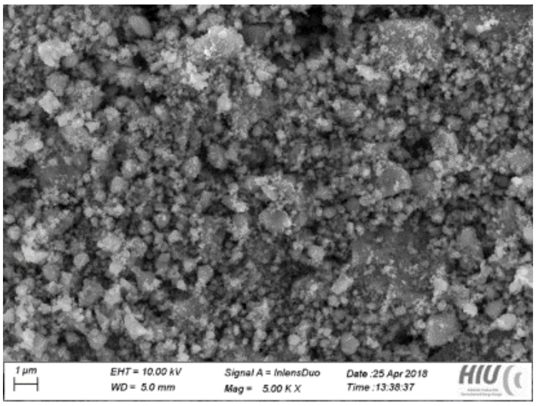

***Figure 1**: SEM images of Li_2VO_2F*

The XRD patterns of the obtained materials are gathered in Figure 2. As expected, the lattice parameters increase with the increase of the atomic radii of the transition metal.

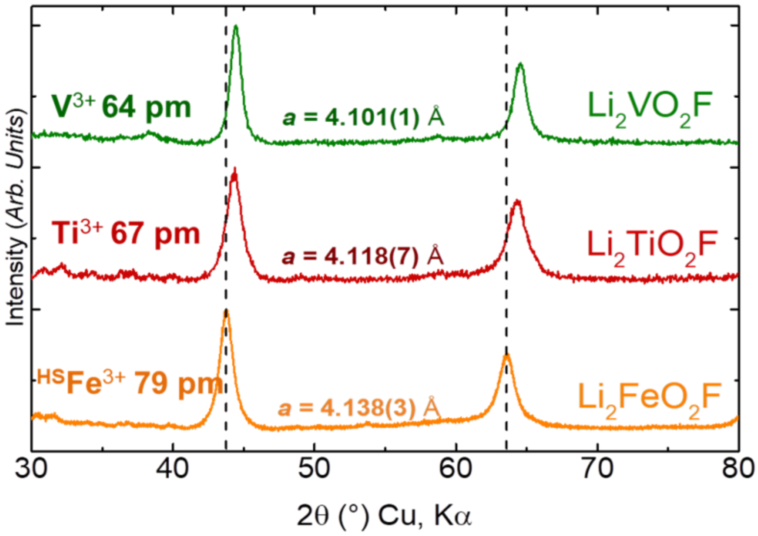

***Figure 2**: XRD patterns of Li_2VO_2F, Li_2TiO_2F and Li_2FeO_2F obtained by mechanosynthesis*

Materials were further characterized by Li MAS NMR (Figure 3). Surprisingly, the chemical shifts were closer to 0 ppm for Li_2VO_2F and Li_2TiO_2F indicating a diamagnetic behavior.

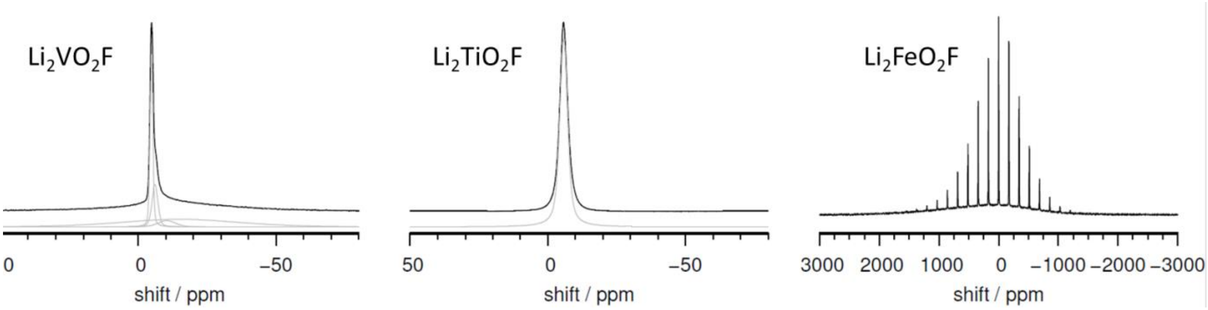

***Figure 3** : 6Li MAS NMR of Li_2VO_2F, Li_2TiO_2F and Li_2FeO_2F*

The static molar magnetic susceptibilities of Li_2VO_2F ($\chi(T) = M(T)/H$ (H = 1 T) with H as the magnetic field and M as the magnetization) were measured between 5 and 300 K using a SQUID magnetometer (Quantum Design) for the two materials. The zero field cooled χ values were obtained by cooling the sample in zero field down to 5 K and then heating them under the measuring field. The diamagnetic contributions were corrected using the atomic values from G.A. Bain and J.F. Berry[1] yielding the paramagnetic susceptibility contribution. The temperature dependence of the χ ratio for $Li_2V^{+3}O_2F$ together with $V^{+5}PO_4O$ and $LiV^{+4}PO_4O$ is gathered in Figure 4. Surprisingly, Li_2VO_2F exhibited no magnetism. More surprisingly, the magnetism of $Li_2V^{+3}O_2F$ is lower than $V^{+5}PO_4O$ for which vanadium valence is +5 with no unpaid electron according to the configuration of V^{+5} (d^0: e_g^0 ; t_{2g}^0). One possible explanation of the diamagnetic behavior of $Li_2V^{+3}O_2F$ might be due to the removing degeneracy in t_{2g} (V^{+3}: d^2: e_g^0; t_{2g}^2) so that the 2 unpaired electrons in t_{2g} become pair after removal of degeneracy.

---

[1] Bain, G.A. and Berry, J.F.; Diamagnetic corrections and Pascal's constants, Journal of Chemical Education, 2008, 85(4): p. 532-536.

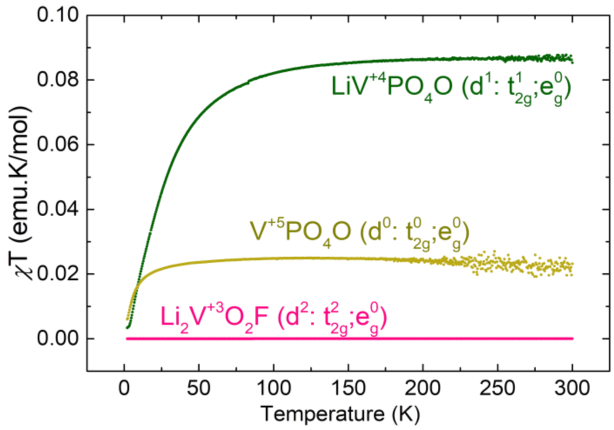

***Figure 4**: Temperature dependence of χT for Li_2VO_2F, VPO_4O and $LiVPO_4O$.*

3.2 Electrochemical Performances Reported by Consortium Patterns

3.2.1 Electrochemical Performances as tested by CEA

The protocol followed by CEA Grenoble for electrochemical testing is the following:

- Same proportion of components is used as at KIT, namely, 75% of coated materials, 15% of carbon black and 10% of PVDF
- The components are mixed using a manual grinding in a mortar
- NMP is used to create an ink with the mixed components
- The ink is casted on an Al foil and doctor-bladed to a thickness of 200 μm (as at KIT), this results in an approximate loading of 2 mg/cm², close to what is achieved in KIT
- The coating is dried and electrodes of 14mm diameter are punched and pressed to 10 T

The coin cell is then cycled at C/20 rate between 1.3 V and 4.1 V in a 1:1 EC/DMC electrolyte containing 1 M $LiPF_6$, according.

In their interim report[2], CEA reported the electrochemical performances of Li_2VO_2F prepared in different batches. The first batch of Li_2VO_2F cathode material was characterized in half cells (cathode//Li). The electrochemical behavior is shown in Figure 5. The open circuit voltage (OCV) is about 2.5 V. Li_2VO_2F delivers a first discharge capacity of 324 mAh/g (at C/20), which is in agreement with previous data published in 2015[3]. The first charge capacity (240 mAh/g) is lower than the first discharge capacity (324 mAh/g). The sloping profiles suggest a single-phase intercalation mechanism.

---

[2] LiRichFCC_D4.3_InterimPerformanceReport

[3] Ruiyong Chen et al. ; Li^+ intercalation in isostructural Li_2VO_3 and Li_2VO_2F with O^{2-} and mixed O^{2-}/Fanions, Phys. Chem. Phys., **2015**, 17, 17288-17295.

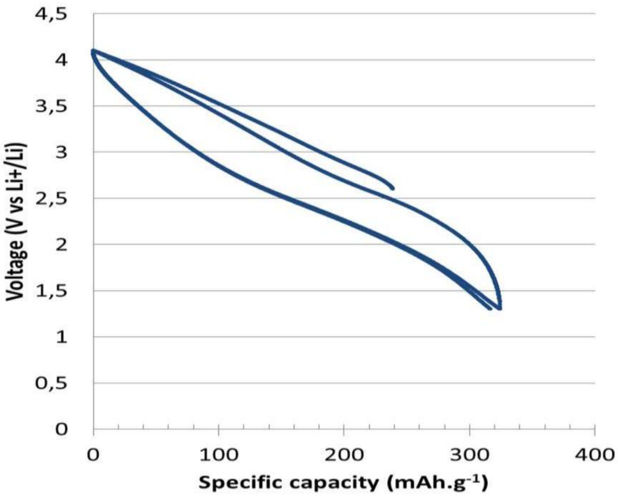

Figure 5: *Voltage profiles of Li_2VO_2F cycled at a current-rate C/20 vs specific capacity (picture from deliverable 4.3)*

It should be noted that there is always a discrepancy between two different cells within a same batch, owing to the mass uncertainty coming from the material deletement (fragile layer). Still, the measurements clearly show that the capacities and energy efficiencies of cells assembled from batch 2 of Li_2VO_2F are better than batteries made from batch 1. The coulombic efficiencies are also better but decrease after 20 cycles of charge-discharge (Figure 6).

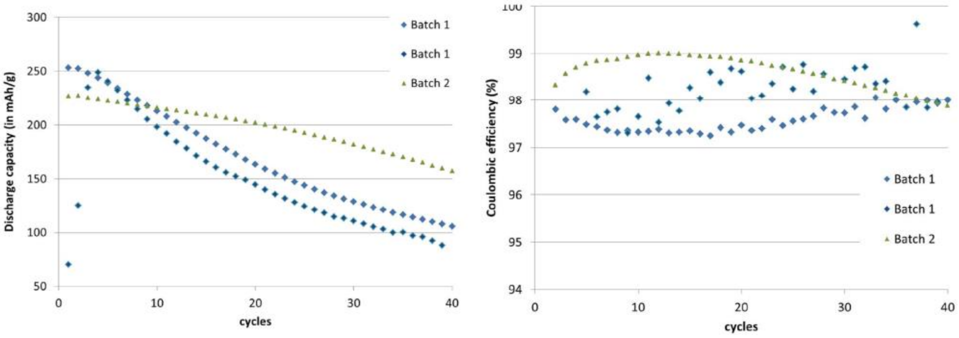

Figure 6: *Discharge capacity (a), coulombic (b) efficiencies vs cycles curves for 2 batches of Li_2VO_2F. (picture from deliverable 4.3)*

3.2.2 Electrochemical Performances of the AlF_3 coated on Li_2VO_2F

The preliminary electrochemical test of Li_2VO_2F performed at KIT, revealed that the Li_2VO_2F material suffers from instability against the electrolyte which leads to important capacity decay during the cycle life. The main goal of Task 2.2 carried in CEA was to provide a protective coating against the undesired interaction with electrolyte thus stabilizing the material's electrochemical performance. Specifically, CEA reported coating of Li_2VO_2F by 1.5 %wt of AlF_3. The performances of this material show a strong improvement of capacity retention during the first 100 cycles compared to the non-coated material tested under the same conditions. The material was then electrochemically tested according to the protocol described previously.

The distribution of the elements in coated material is rather homogeneous. Especially Al is found all over the surface of the material (Figure 7). As the pristine rock-salt also contains F, the presence of F in the coated material cannot be easily interpreted.

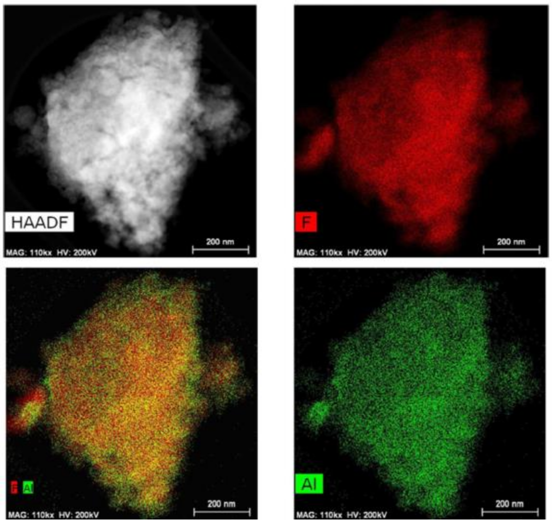

***Figure 7**: TEM-EDX mappings of the 1.5wt% AlF_3-coated material.*
(Picture from deliverable 2.2)

The electrochemical observations reveal that the presence of the coating strongly reduces the capacity at the first cycle (Figure 8). This may be due to the resistive behavior of this coating and might be optimized by reducing the thickness of the coating. However, the behavior during cycling life is much more stable in the case of the coated material. After 100 cycles the discharge capacity of coated material is 85.2mAh/g (42% capacity retention) compared to 44.8mAh/g (15% capacity retention) for the uncoated reference, i.e. the presence of coating almost doubles the capacity retention. This validates that the coating helps stabilize the material during cycling. However, the coulombic efficiencies remain insufficient, potentially indicating instability of the electrolyte on the material and/or coating surface.

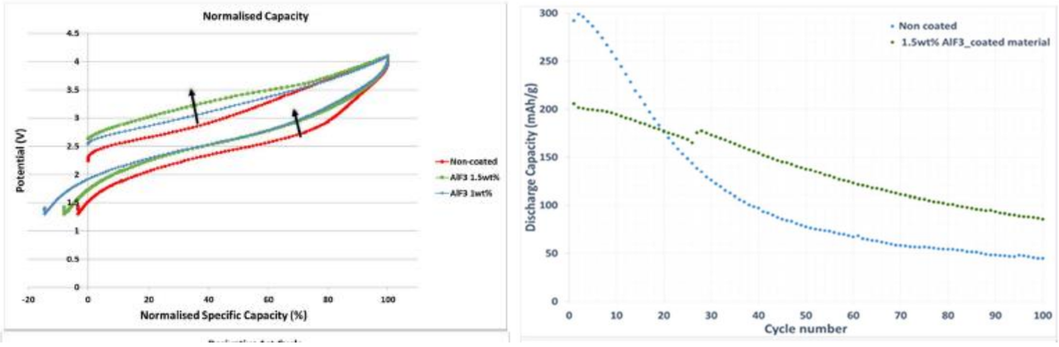

***Figure 8**: (left) Evolution of the electrochemical profile of 1st cycle with the amount of coating.*
(right) Discharge capacity vs. number of cycles of the uncoated and coated Li_2VO_2F.
(picture from deliverable 4.3)

3.3 Dynamics of Li+ in the material / Interfacial transport

The result of a NEB calculation on a Li vacancy diffusing in the nearly fully lithiated phase, $Li_{1.94}VO_2F$, is shown in Figure 9. From there, an activation barrier of 0.54 eV is found for the jump of 2.83 Å between the nearest-neighbor sites. The Li passes through a neighboring OF_3 tetrahedron instead of the other option, namely a neighboring O_3F tetrahedron, indicating that F-rich tetrahedra are the preferred Li diffusion channels in the fully lithiated phase. The corresponding Li diffusivity is $1.92 \cdot 10^{-11}$ cm^2/s (using a vibrational frequency of 10^{13} s^{-1}), which is in rough agreement with experimental values (10^{-9} cm^2/s).

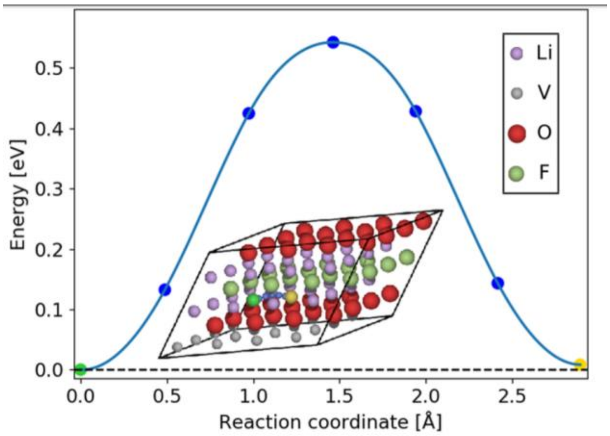

Figure 9: *NEB profile for the activation barrier for a Li vacancy diffusing in the nearly fully lithiated phase of $Li_{1.94}VO_2F$. The initial and final positions are presented by the green and yellow atoms, respectively, and the intermediate positions are indicated by the blue atoms. (picture from deliverable 3.1)*

In general, we find that the diffusion barrier strongly depends on the local environment. As expected, the divacancy mechanism results in significantly reduced diffusion barriers. However, if the di-vacancy concentration in the compound is low, the associated divacancy jump mechanism is not activated, and the Li diffusion can only proceed via the direct mechanism. In this direct-jump case, the 0-TM barrier is slightly lower than the 1-TM.

3.4 EIS of the Li_2VO_2F: before and after coating

The electrochemical tests were performed in a Swagelok cell assembled in an argon-filled dry glove box. Prior to the use, the active materials were ball milled with 15 wt % of C65 (from TIMCAL) and 10% wt of PVdF-HFP was added in the obtained powder. PVdF-HFP was applied as a solution of 10% wt of PVdF-HFP and 90% wt of NMP. In order to ensure porosity and rapid electrolyte uptake within the electrodes, 33 wt % of Dibutylphtalate (DBP) was added[4]. Finally, some drops of NMP were added for appropriate viscosity, and the slurry was stirred for 2 hours prior to be casted on a glass plate using a doctor blade technique (with a GAP of 500 µm). After drying, electrodes of 12 mm in diameter were cut and pressed together with Al-mesh disk. The obtained electrodes were soaked in diethyl ether in order to remove DBP. The electrode loadings were between 3-4 mg/cm^2. The cells consisted of the positive electrode (as described above), Li disk as a negative electrode, and 1 M of LiPF6 in a mixture of EC-DEC (1:1) as electrolyte (LP40). The assembled cells were cycled between 4.1 V and 1.3 V *vs.* Li^+/Li.

---

[4] A. S. Gozdz, C. Schmutz, and J.-M. Tarascon, “Rechargeable lithium intercalation battery with hybrid polymeric electrolyte,” US Pat., vol. 5 296 318, 1994.

3.4.1 Electrodes degradation due to ageing

Electrochemical performances of Li_2VO_2F were evaluated in different time frames as demonstrated in Figure 10. The aged electrodes are directly linked to the poor capacity of the materials. Moreover, the EIS spectra displayed in Figure 11 indicate an increase of the amplitude of the EIS with time. However when new electrodes are built from aged Li_2VO_2F, no capacity fading is observed.

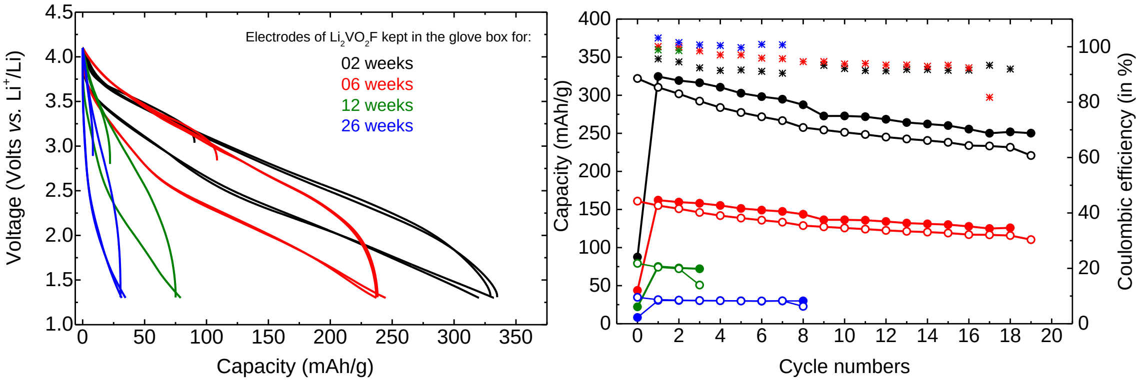

***Figure 10**: (left) Voltage vs. Capacity of Li_2VO_2F at different time frame (right) charge capacity (close dots) discharge capacity (opend dots) coulombic efficiency (stars)*

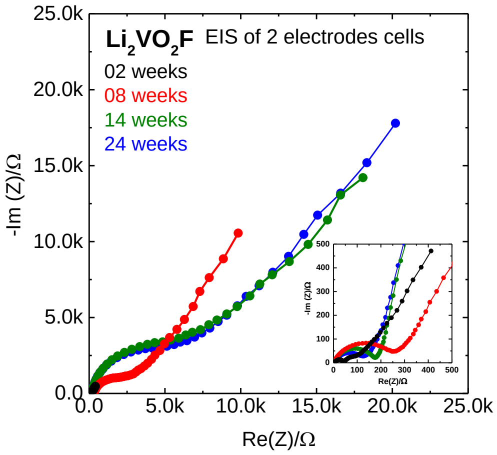

***Figure 11**: symetrical EIS of two electrodes cell of Li_2VO_2F at different time frame*

3.4.2 Effect of electrolyte concentration

In the next set of experiments, we carried out EIS measurements on three equal Li_2VO_2F cathode materials but using three different concentrations of LiPF6 in EC/DEC (1 M, 0.1 M and 0.01 M in EC/DEC:1/1). The change in electrolyte concentration causes big changes in the magnitude of impedance, so the graphs are shown at different magnifications (

Figure 12).

The decrease in concentration especially affects the size of the medium frequency arc. This is in line with assumption that this arc represents the parallel combination of charge transfer resistance and double layer capacitance, similarly as found in our previous investigation of a $LiCoO_2$ material[5]. By contrast, the low-frequency (LF) capacitive part is more or less independent of the concentration of electrolyte. This means that LF is not associated with electrolyte phenomena such as diffusion of mobile species in electrolyte-filled pores etc. Rather, this part (LF) corresponds to transport inside the active particles. This is highly important to know as this part has the highest impedances (in most cases of interest) and determines the overall transport in the whole electrode material).

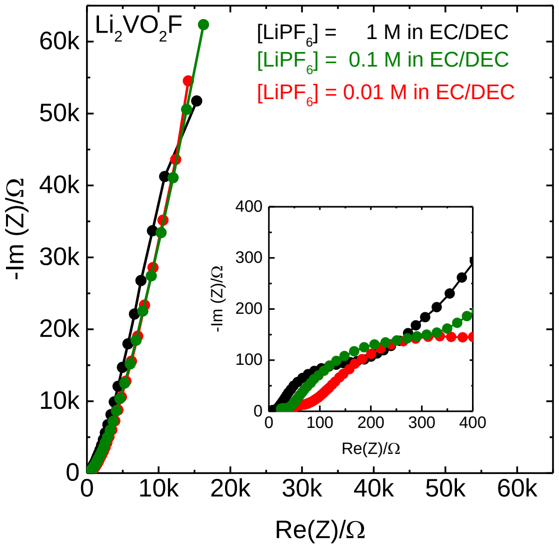

Figure 12: Measured EIS spectra of three Li_2VO_2F-based symmetrical cells with the same electrode composition. The spectra was measured from 1MHz-10 µHz. Black line, green line and red line are for 1 M, 0.1 M and 0.01 M concentrations of $LiPF_6$ salt in EC:DEC = 1:1 by volume.

3.4.3 EIS upon charge/discharge

The evolution of the EIS upon charge and discharge of Li_2VO_2F in half cell was study as follows:

- The cell was charged/discharged three times at C/20
- During the 4th cycle, the cell was charged every hour, relaxed for 5 hours and then EIS measured from 20 kHz down to 0.1 mHz.

The obtained galvanostatic curves and all the EIS measurements are collected in Figure 13.

Upon charge (from 1.3 V up to 4.1V) the medium frequency (MF) arc increases and on subsequent discharge, the MF arc decreases. Although reversible, the process is not symmetric *e.g.* the size of the arc at a particular potential upon charge has different dimension compared to the same potential upon discharge (Figure 14). However, the EIS are symmetric with respect to composition e.g. the sizes of the arc at a particular electrode material composition are similar for all cases (*Figure 15*).

---

[5] J.M. Ateba Mba; J. Moskon; S. Pejovnik; M. Gaberšček; *Journal of The Electrochemical Society,* **2010**

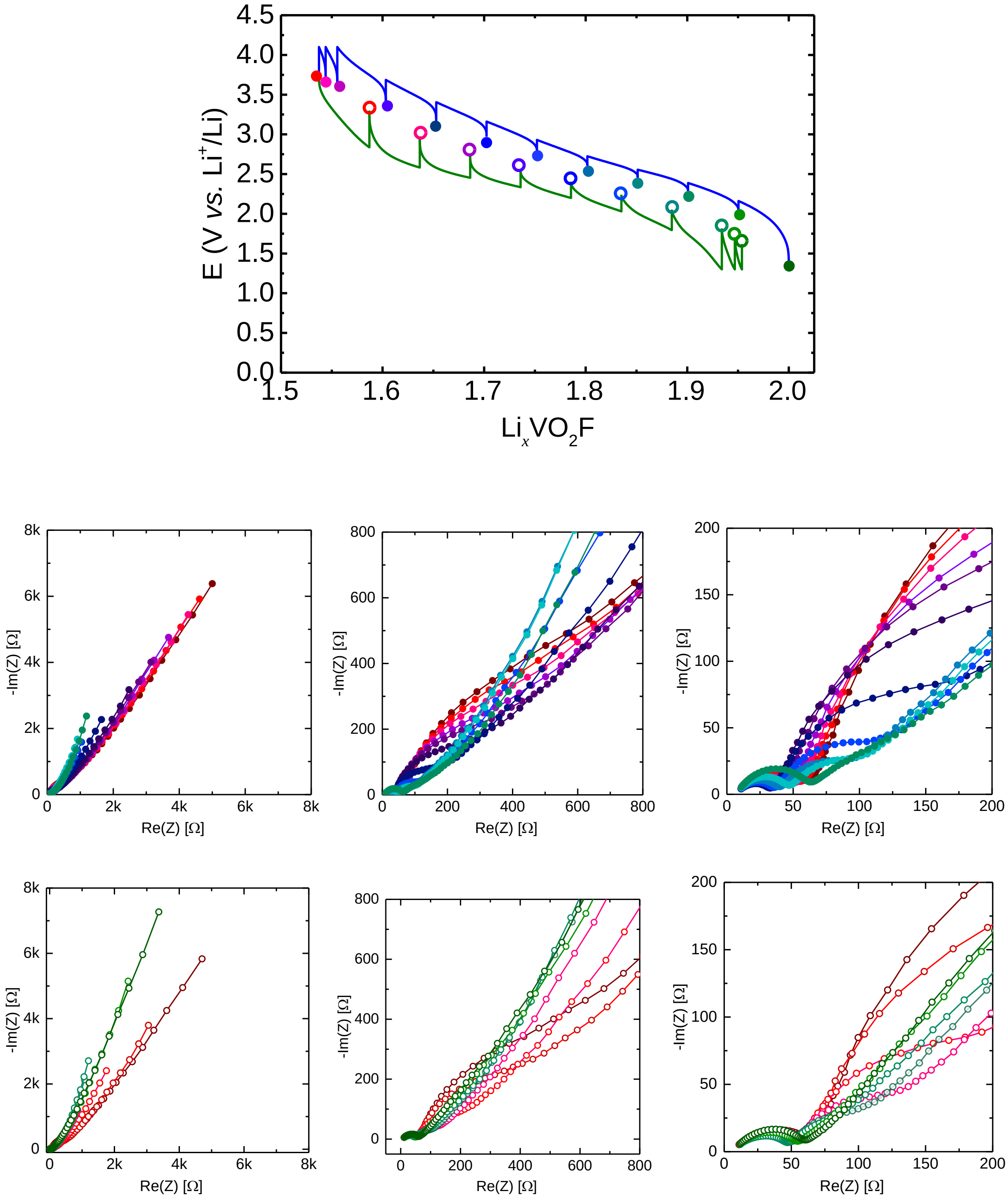

Figure 13: (top) GITT-type curve of Li_2VO_2F; the dots represent the points where EIS spectra were collected. (middle) EIS spectra on charge (bottom) EIS spectra on discharge

At higher voltages, the MF arc and the diffusional tail overlap forming a beginning of a big semi-circle. Note that the MF arc is connected to charge transfer resistance, as shown above. The increase of the MF arc means the charge transfer resistance is inhibited but still present at higher voltage. This indicates the inability to extract all the Li+ from the structure as already demonstrated by DTU[6].

At lower voltages, the MF decreases and finally disappears whereas diffusional tail appears within the same frequency range. Those changes occur at potentials below 2.29 V. In other

---

[6] LiRichFCC_D3p1_Preliminary_transport_report

words, especially below 2.29 V the diffusion impedance largely prevails over the charge transfer impedance.

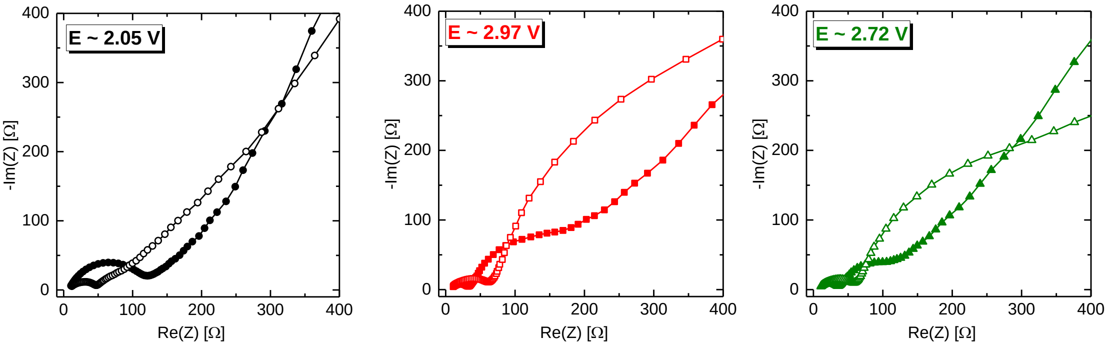

***Figure 14**: EIS of the “cathode-Li” cell of Li_2VO_2F at the same relax potentials on charge (full dots) and discharge (open dot).*

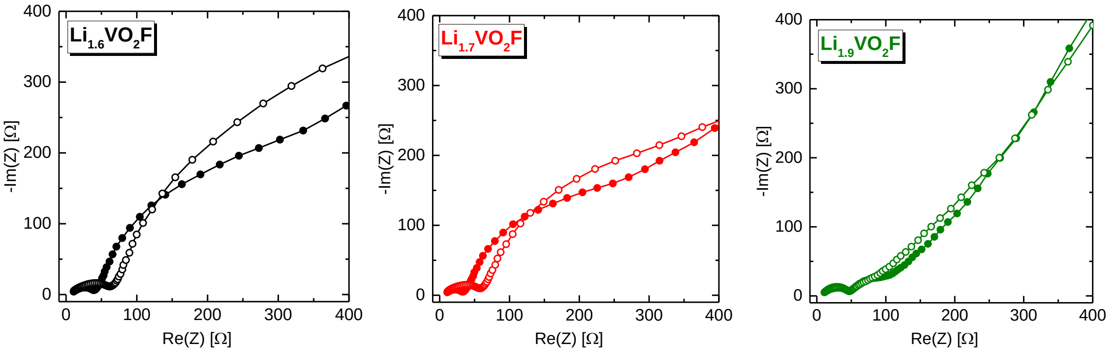

***Figure 15**: EIS of the “cathode-Li” cell of Li_2VO_2F at the same composition of Li_2VO_2F on charge (full dots) and discharge (open dot).*

3.4.4 Charge transfer resistance vs. Cycle numbers

The galvanostatic behavior (at C/20 from 1.3 V to 4.1 V) of every 10th cycle of Li_2VO_2F is displayed in Figure 16. The estimated operating potential is 2.7 V. We measured the EIS spectra at that potential on charge and on discharge according to the galvanostatic curve in Figure 17.

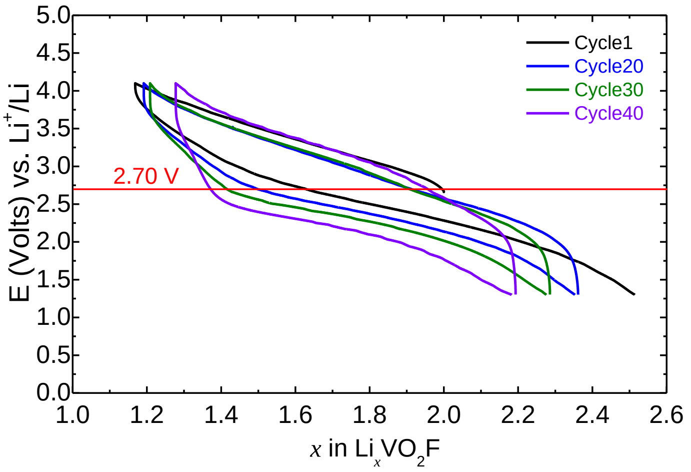

***Figure 16**: Galvanostatic behavior of Li_2VO_2F at every 10th cylce.*

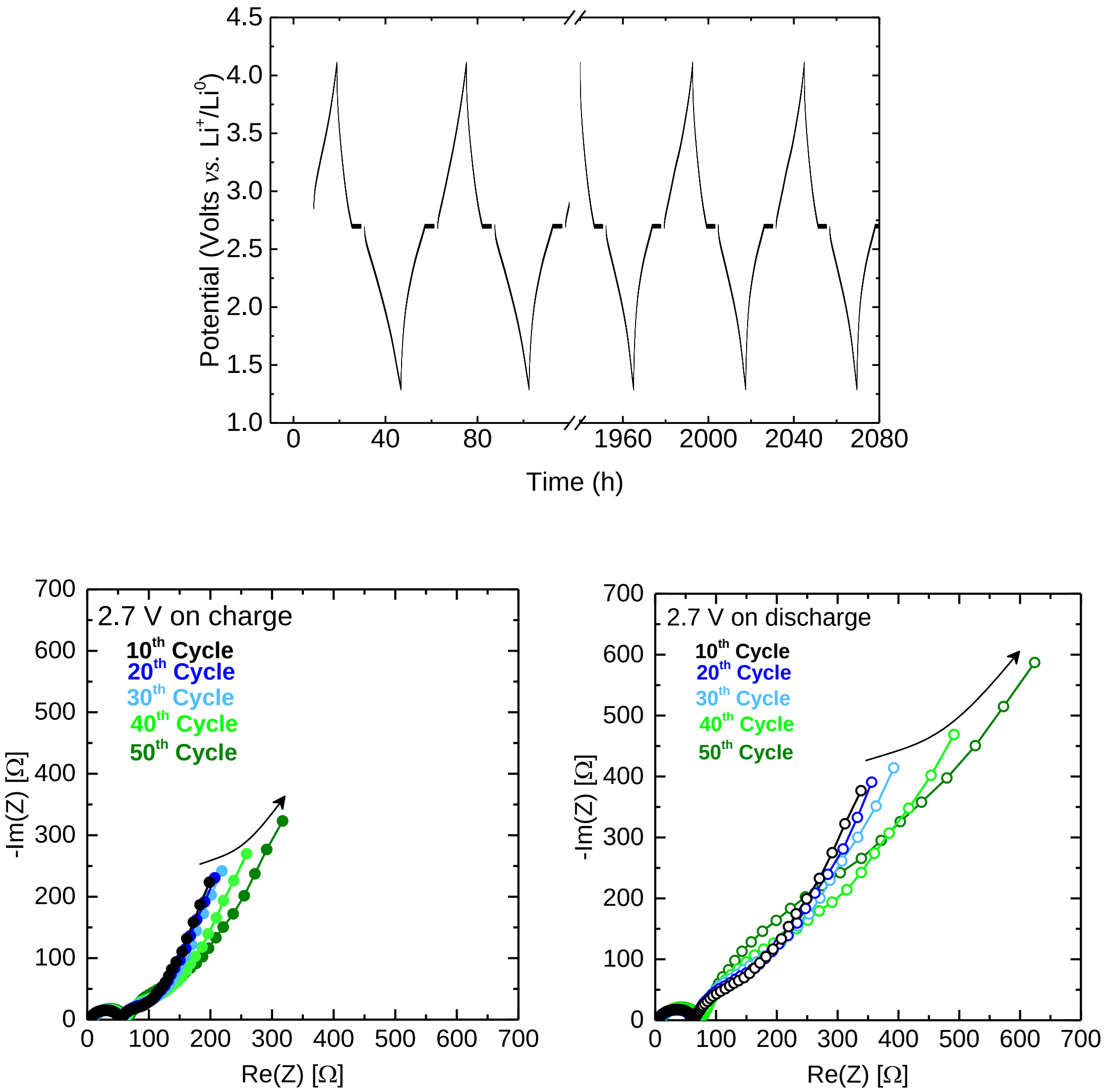

***Figure 17**: (top) Galvanostatic behavior with a potential hold at 2.7 V.*
(bottom left) EIS spectra on charge at 2.7 V. (bottom right) EIS spectra on discharge at 2.7 V

At given potential, the amplitude of EIS is higher on discharge than on charge. Similarly, the MF arc (charge transfer resistance) is higher on discharge. Figure 17 shows that the resistance of the cell is higher on discharge. This seems to indicate that the incorporation in of Li+ in Li_2VO_2F is hindered on discharge. Figure 16 indicates that upon cycling the polarization is increasing with the increase of cycle number. More interestingly, that increase occurs mainly on discharge whereas the operating voltage on charge is almost constant.

The fact that it is easier to extract Li^+ from Li_2VO_2F than to insert it comes from the intrinsic structure of the material. Indeed, one might hypothesise that during the charge it is easier to extract Li^+ due to Li percolation. However during insertion we are incorporating Li^+ in site structure which contained either V or Li. The repulsion may hinder the insertion of Li^+.

3.4.5 Coated Li_2VO_2F

EIS was measured on the Li_2VO_2F coated with 1.5 %wt of AlF_3 coated Li_2VO_2F. The electrodes were provided by CEA. The EIS of two-electrode cell of Li_2VO_2F before and after coating are recorded in Figure 18a. One can notice the absence of the MF arc in the coated Li_2VO_2F. In order to check whether it is an absence or a significant reduction of MF arc, a symmetrical cell on both materials was prepared and the results gathered in Figure 18b. Now we clearly reveal the presence of the MF arc which is actually two times smaller than for the uncoated Li_2VO_2F.

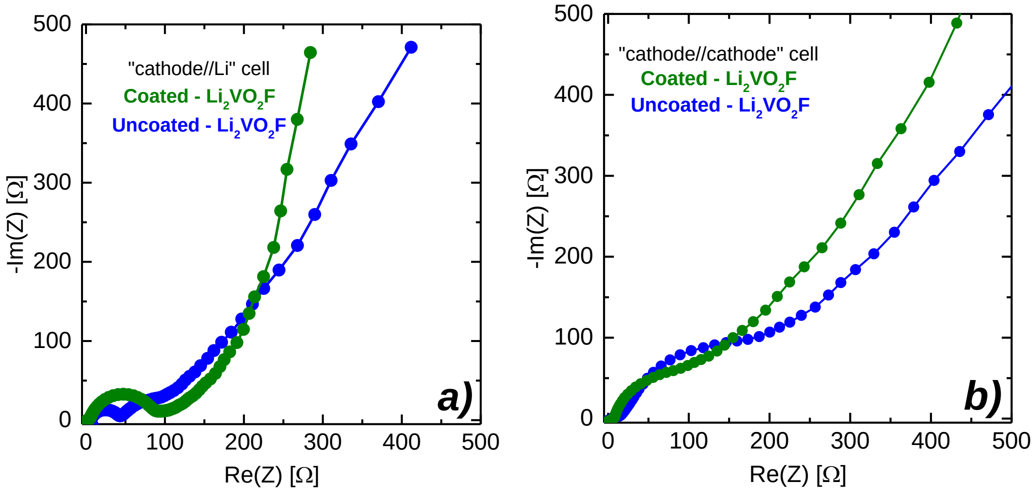

<u>Figure 18</u>: (a) "cathode//Li" cell of Li_2VO_2F before and after coating. (b) "cathode//cathode" cell of Li_2VO_2F before and after coating.

The evolution of the EIS upon charge and discharge of AlF_3-coated Li_2VO_2F in half cell was studied as follows: the cell was charged during 2 hours and relaxed for 4 hours, then the EIS was measured from 1 MHz down to 1 mHz. The galvanostatic curve obtained is recorded in Figure 19 and all the EIS spectra are collected in Figure 20.

During the charge the amplitude of the EIS spectra is increasing. Contrary to the non-coated Li_2VO_2F, where we observed a beginning of a big semi-circle, here there is absence of such a feature.

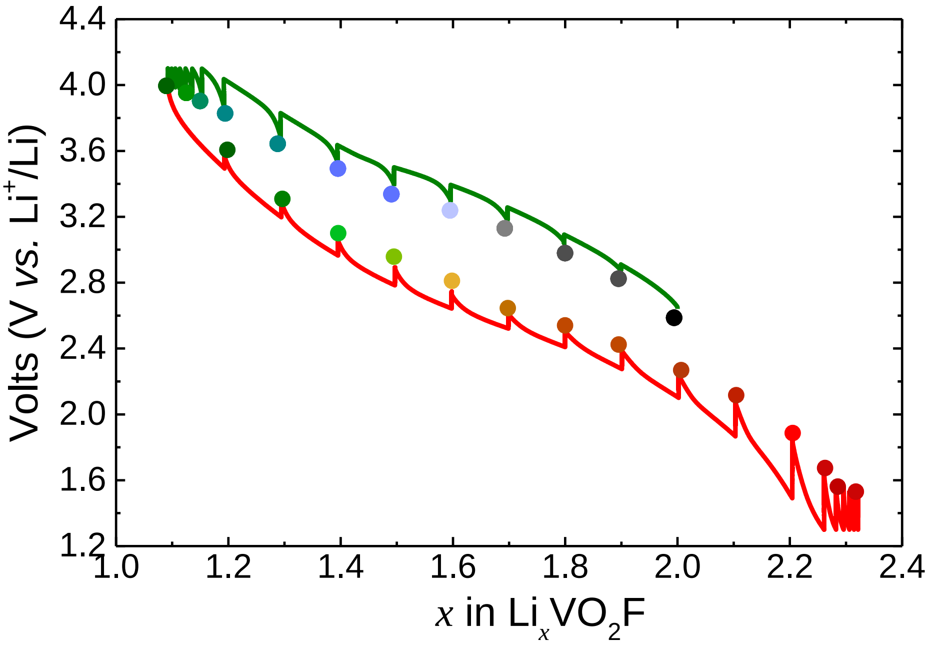

***Figure 19**: Galvanostatic curve of the coated Li_2VO_2F: The cell was charge/discharge for 2 hours and relaxed for 5 hours before the measurement of EIS spectra.*

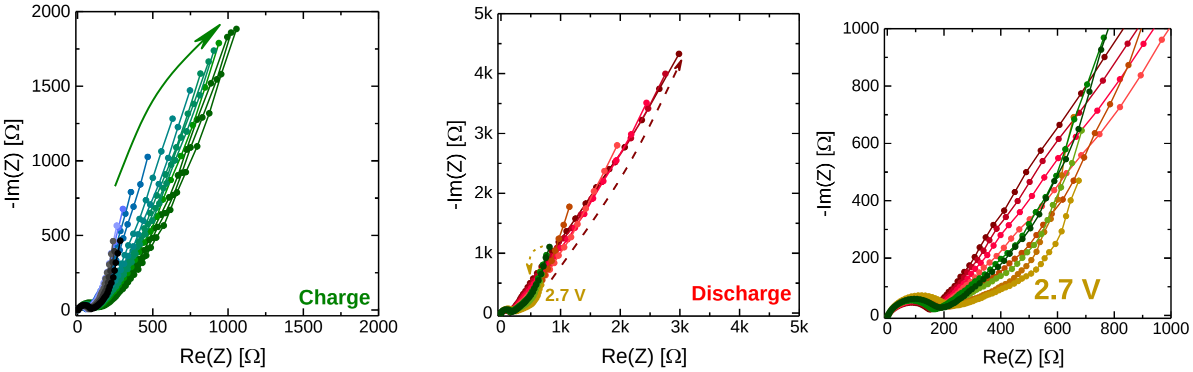

***Figure 20**: EIS spectra of the coated Li_2VO_2F during charge (left) discharge (middle) and zoom of the spectra at the discharge (right)*

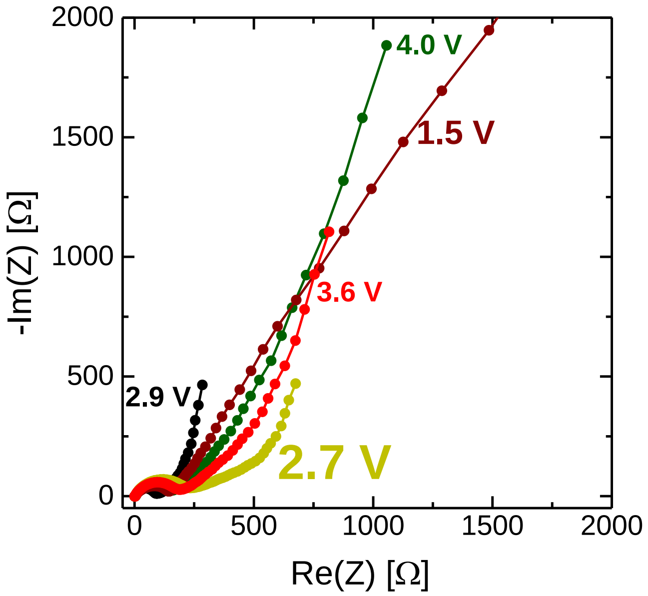

Figure 21: *Potential selective EIS spectra of the coated Li_2VO_2F.*

During Li^+ insertion (from 4.1 V), the amplitude of the EIS decreases up to a potential of 2.7 V. At that potential the amplitude reaches a minimum value (Figure 21).

3.5 EIS of Li2FeO2F

The evolution of EIS spectra upon charge and discharge of Li_2FeO_2F in half cell configuration was studied as follows: the cell was charged during 2 hours and relaxed for 4 hours, and then the EIS spectra were measured from 1 MHz down to 1 mHz.

The galvanostatic curve obtained is displayed in Figure 22 and all the EIS spectra are collected in Figure 23. Close to the OCV, the EIS at low frequency is inclined at 45 °, which is characteristic of Warburg diffusion. At low voltages, the EIS at low frequency is almost parallel to the imaginary axis. During subsequent charge, the EIS at low frequencies again becomes inclined at 45 °.

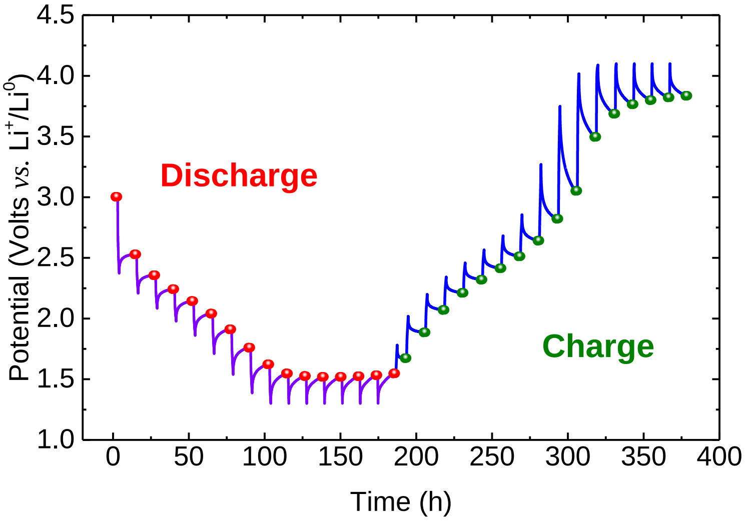

Figure 22: *GITT type cycle of Li_2FeO_2F the EIS was measured after the relaxation.*

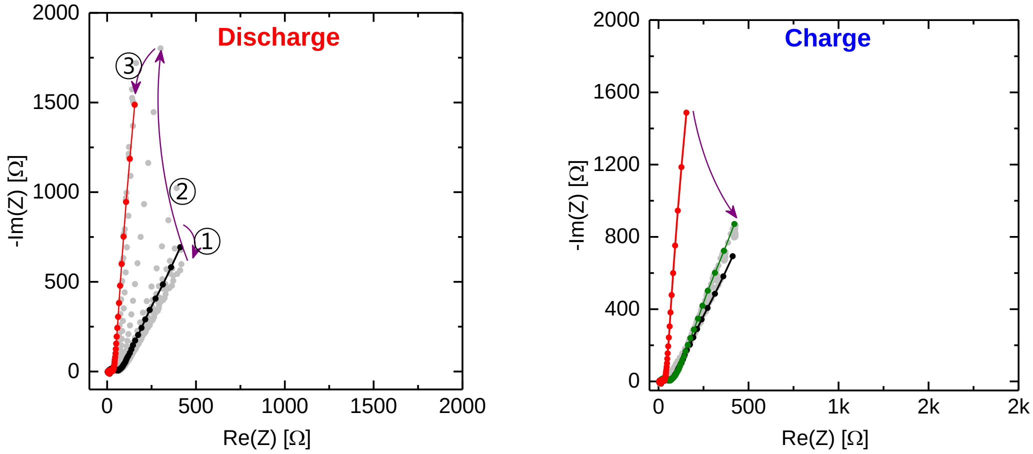

Figure 23: *EIS spectra of Li_2FeO_2F during charge (left) and discharge (right).*

Six half-cells with electrode corresponding to the potential of 2.4 V (Figure 24) were assembled. The EIS spectra of the resulting three symmetrical cells constructed from those 6 electrodes were measured. Each cell contained a different electrolyte concentration (Figure 25).

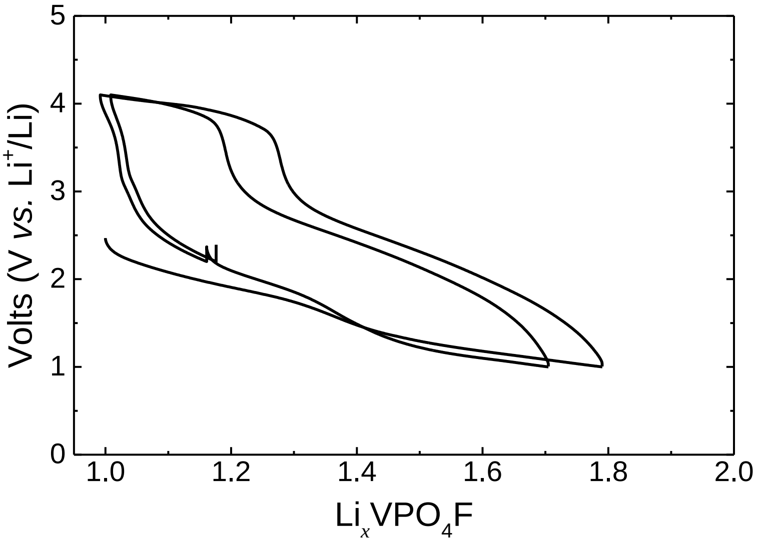

Figure 24: *Two galvanostatic curve of Li_2FeO_2F at C/20. The cell was stopped at 2.2 V and relaxed for 10 hours.*

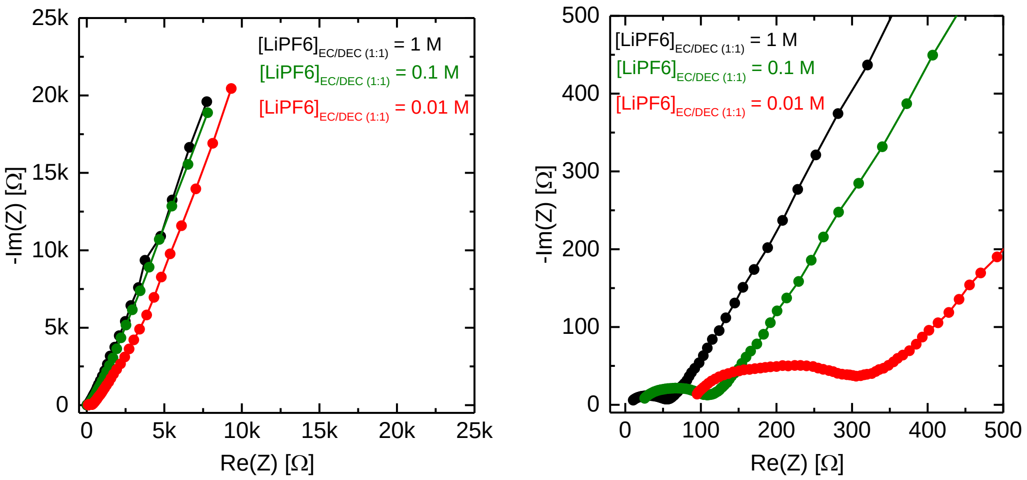

Figure 25: *Symmetrical cell of Li_2FeO_2F with different electrolyte concentration. The electrodes were pre-cycled as shown in Figure 24*.

Again, the concentration has no effect on the low-frequency part (inclined slopy feature corresponding roughly to Warburg impedance in combination with capacitive behaviour). This independence strongly indicates that this high-impedance part corresponds to an area that does not involve electrolyte, i.e. the inner of active particles. In other words, the overall transport-reaction impedance is determined by the slow diffusion of charge inside active particles (and not, for example by charge transfer or by transport in electrolyte or by contact issues etc.). By contrast, the interfacial phenomena (charge transfer, coating resistance etc.) and, potentially, diffusion in liquid electrolyte in electrode pores are visible at intermediate frequencies (see the extended semicircles which grow in size from black to green to red in Fig. 25). However, at usual concentrations (black curve) the impedance of this arc is very small (less than 70 Ohm) so this part does not represent significant limitation to the cell operation.

We can do further analysis of the diffusional part of the spectra (Figure 25) by shifting the real part of impedance of the two spectra for 0.1M and 0.01M $LiPF_6$ concentration as shown in Figure 26. Thus we find that roughly bellow 0.16 mHz the spectra are very similar (within the error of electrode mass determination) what additionally confirms that the slowest process (solid state diffusion) is indeed independent of Li salt concentration in electrolyte.

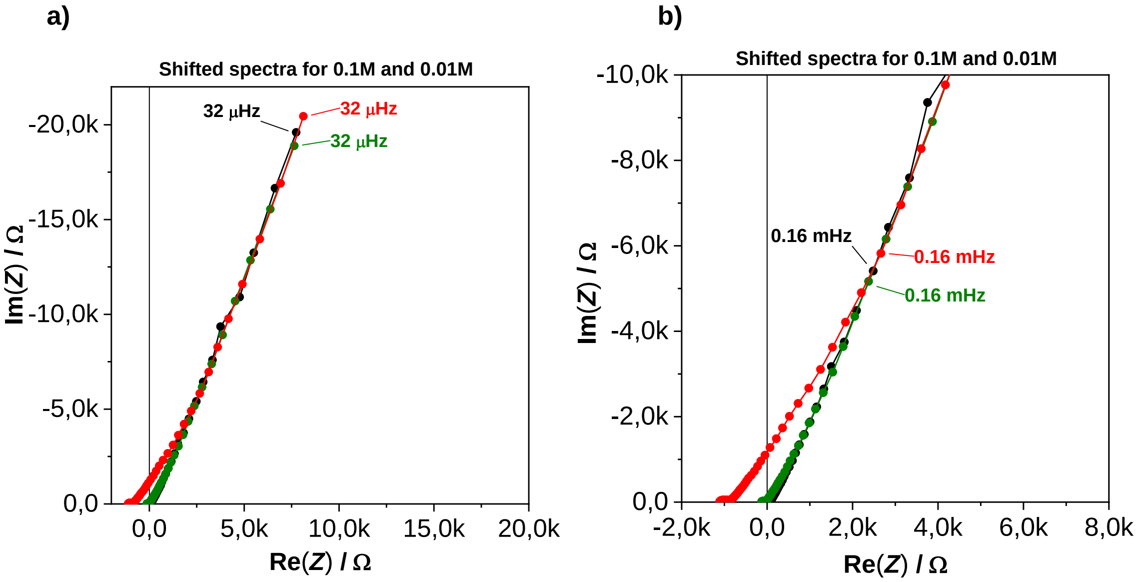

***Figure 26**: Measured impedance response of symmetrical cells based on Li2FeO2F with different electrolyte concentrations, where the real part of data (Re(Z)) for cells with 0.1 M and 0.01 M were shifted to lower values in order to obtain matching with the low-frequency data measured on cell with 1 M electrolyte.*

Furthermore, we can directly correlate the measured impedance data with galvanostatic cycling. We read out value of voltage hysteresis in central region at the inflection points in the corresponding voltage curves (Figure 27a) and divide it by the current difference (2-times the applied current for galvanostatic experiment). This means we obtain value of the total cell resistance, R_{cell}, in the central region. In the particular case of the analyzed Li_2FeO_2F–Li half-cell we obtained R_{cell} to be 4720 Ω. In order to compare this with the impedance response of symmetric Li_2FeO_2F–Li_2FeO_2F cell we multiply it with two to take into account the two Li_2FeO_2F electrodes that are in series with respect to the resulting energy (voltage) loss. In the measured impedance spectrum of Li_2FeO_2F–Li cell with 1 M electrolyte concentration we read out the closest value of impedance modulus, $|Z|$, that matches the most with $2\times R_{cell}$. As shown in Figure 27b the correlated frequency is roughly 80 μHz what corresponds to about 3.5 hours. This finding is very important because we can directly see in the Figure 27b that the magnitude of impedance response after the frequency of 80 μHz (this means at even lower frequencies) is still growing equally both in Re(Z) and -Im(Z). Based on that we can conclude that probably whole of the galvanostatic charge and discharge sequence of Li_2FeO_2F are controlled by increasingly growing diffusional impedance of the cell. From the practical point of view it follows that the full capacity of Li_2FeO_2F system cannot be achieved due to the fact that we have too long diffusion paths (too large particles) which cannot be fully utilized for reversible storage of lithium/energy in time scales used in practical battery applications.

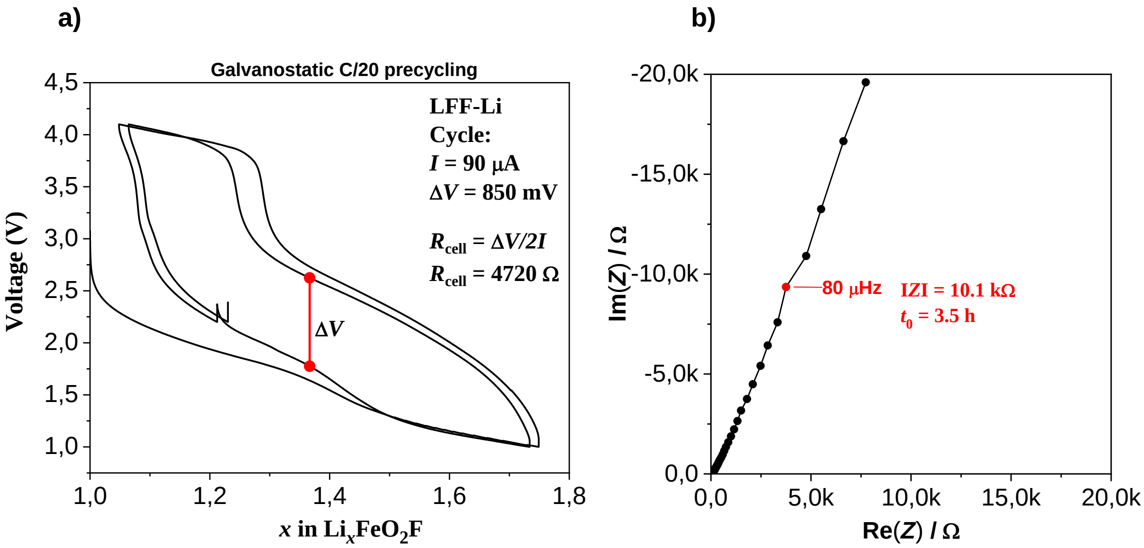

Figure 27: *a) Reading out of voltage hysteresis in central region of galvanostatic C/20 cycle measured on Li_2FeO_2F–Li cell and obtaining of the corresponding total cell resistance (R_{cell}). b) Measured impedance response of symmetric Li_2FeO_2F–Li_2FeO_2F cell with marked point (80 µHz) that matches best with the galvanostatic cycle ($|Z| \approx 2 \times R_{cell}$).*

3.6 EIS of Li_2TiO_2F

The evolution of the EIS upon charge and discharge of Li_2TiO_2F in half cells was studied as follows: the cell was charged during 30 minutes at C/20 and relaxed for 5 hours, after which the EIS was measured from 1 MHz down to 1 mHz.

The galvanostatic curve obtained is displayed in Figure 28 and all the EIS spectra are collected in Figure 29. Close to the OCV, the EIS at low frequency is almost parallel to imaginary axis characteristic of blocking electrode (dominating by the capacity of interfaces without significant bulk storage being indicated). Indeed after 30 min on charge the potential was 4.1 V – namely, no battery capacity during charge was observed. At higher voltages, the EIS at low frequency is almost parallel to the imaginary axis and the amplitude of the EIS is constant. At subsequent charge, the amplitude of the EIS spectra is decreasing. The minimum EIS spectra were recorded for a potential of 2.2 V which is the operating potential of the Li_2TiO_2F material in Li-ion battery.

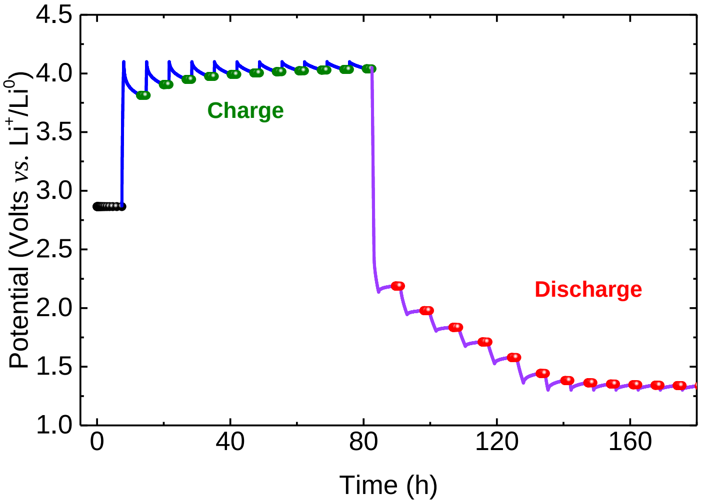

Figure 28: *GITT type cycle of Li_2TiO_2F the EIS was measured after the relaxation*

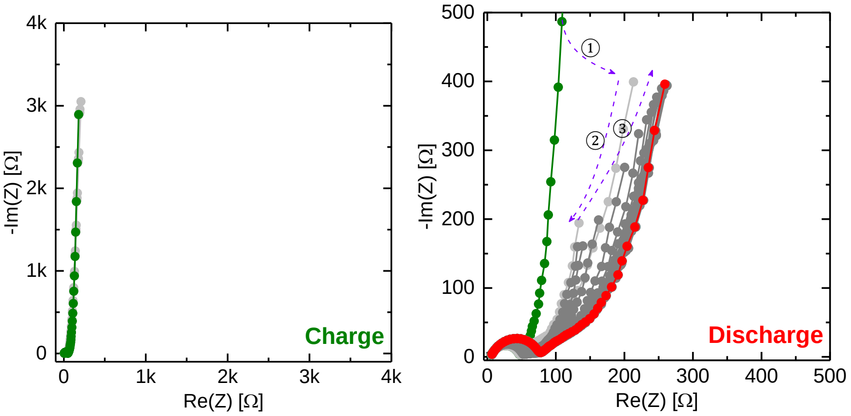

Figure 29: *EIS spectra of Li_2TiO_2F during charge (left) and discharge (right).*

As shown in *Figure 30*, the EIS spectra of Li_2TiO_2F and Li_2VO_2F are very similar at their respective operating potentials. However, one can notice that at lower frequency, the EIS spectrum of Li_2TiO_2F is almost parallel to imaginary axis whereas for Li_2VO_2F, the EIS spectrum is characteristic of Warburg diffusion (*e.g.* inclination at 45 °).

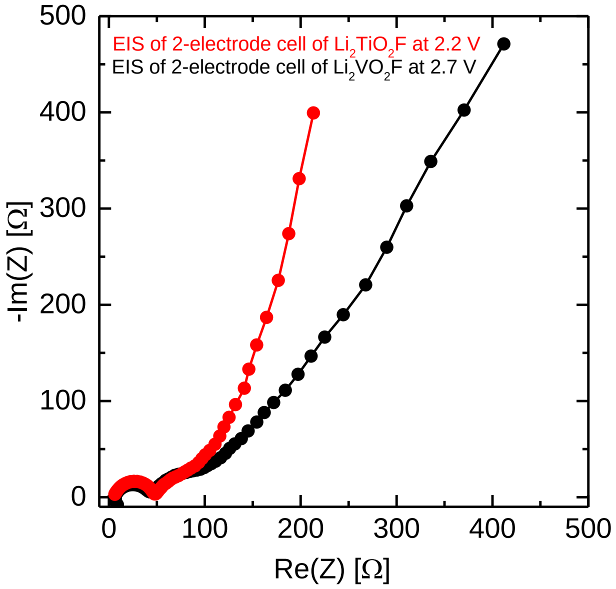

Figure 30: *EIS spectra of Li_2TiO_2F and Li_2VO_2F at their respective operating potential*

4 OUTLOOK

In continuation the qualitative interpretation of EIS spectra for different cases of interest will be upgraded with a quantitative model using the transmission line approach.

5 LIST OF ABBREVIATIONS AND ACRONYMS

EIS: Electrochemical Impedance Spectroscopy
NEB: Nudged Elastic Band
GITT: Galvanostatic Intermittent Titration Technique
LF: Low Frequency
MF: Medium Frequency